MINAR International Journal of Applied Sciences and Technology
ISSN: 2717-8234
Article type: Research Article

Received: 24/05/2023 **Accepted:** 17/06/2023 **Published:** 01/09/2023

SYNTHESIS AND CHARACTIZATION OF TITANIUM DIOXIDE PAPERED BY SPRAY PYROLYSIS AS NO2 AND H2S GAS SENSOR

M. Abd SHAHOODH[1]

Anbar Directorate of Education, Iraq

F. T IBRAHIM[2]

University of Baghdad, Iraq

S. GUERMAZI[3]

University of Sfax, Iraq

Abstract

Titanium Dioxide nanostructures have been prepared by spray pyrolysis technique. It has been characterized using X-ray diffraction, Field emission scanning electron microscopy (FESEM), as well as optical and electrical techniques. The results show that, by analyzing the surface structure through X-ray diffraction and FESEM, the nanoparticles are tiny, spherical, and the particle size is about 21.39-39.93 nm. The uv-vis observed the edge of absorbance at about 375 nm, absorbance in this region is due to the formation of Titanium dioxide nanoparticles, and the energy band gap was determined at 3.3 eV. The gas response of the tested devices towards nitrogen dioxide (NO2) and hydrogen sulfide (H2S) gases in dry air at different operation temperatures. It has been carried out showing a selectivity towards NO2 with sensitivity up to 51.1% at temperatures 300 °C, while the higher sensitivity to H2S gas is about 52.4%.

Keywords: *TiO2, Gas Sensor, Sensitivity, H2S, NO2.*

http://dx.doi.org/10.47832/2717-8234.16.5

[1] mhmdbdshahwdh@gmail.com

[2] Fuad.ibrahim@sc.uobaghdad.edu.iq

[3] samir.guermazi@gmail.com

Introduction

Gas sensors are essential in the detection, monitoring, and control of dangerous and deadly gases that can exist in the atmosphere at very low quantities. Thin-film semiconductor gas sensors are extremely sensitive and trustworthy, with a performance/price ratio similar to that of microelectronic components. Due to their beneficial characteristics, such as a wide bandgap approximately 3.2 eV, a low resistance, and good catalysis, titanium dioxide (TiO2) semiconductive materials have been investigated intensively as chemical sensors for a long time [1]. Due to their high electric conductance, great transparency to visible light, and strong contact with the gas molecules, TiO_2 nanostructures exhibit high gas sensing response. They also have a high surface-to-volume ratio and enormous surface activities[2]. Titanium Dioxide, an n-type degenerate semiconducting oxide, has been used as an ingredient in toothpaste, sunscreen, and polymeric binders. Applications of TiO2 for environmental cleanup, energy production, and biomedicine have attracted more interest recently [3]. For the past three decades, a lot of researchers have written on the physical characteristics of TiO2 films created by various deposition techniques, like laser deposition[4], molecular beam epitaxy[5], chemical vapor deposition[6], electron beam evaporation [7], dc/rf magnetron sputtering[8], electrochemical deposition[9], sol–gel process[10], spray pyrolysis[11], was employed to prepare Titanium Dioxide films in order to suit modern scientific and technological demands.

The present investigation aims to fabricate and characterized the structure, electrical and optical as chemical gas sensing device. The gas sensor fabricated for this study uses Titanium Dioxide as sensing material for monitoring nitrogen dioxide and hydrogen sulfide.

Experimental details

Sigma-Aldrich Titanium chloride (Ticl3) solution about 15% of 99.99 % purity and molecular weight equal to 154.22 g/mole), was also used, without additional purification. The nanostructure thin film is created using the spray pyrolysis technique. 10 milliliters of deionized water were used with 10ml titanium chloride and stirring for five minutes. Glass substrate with 2×2 cm2 dimensions was professionally cleaned to remove any dirt and stains from its surface.

It can be related to the fact that "crystallite size" is not synonymous with "particle size" in the Scherrer equation, although X-Ray diffraction is sensitive to the crystallite size inside the particles. The average crystallite size, D, is calculated using the well-known Scherrer formula: $$D = K\lambda/\beta\cos\theta \quad (1)$$

where λ X-ray wavelength is expressed in nanometers (nm), β peak width at half maximum height due to tiny crystallite size is expressed in radians, and K is a constant related to crystallite structure that is typically taken to be 0.9.

The sensitivity S of a sensor is its reaction to the presence of a certain gas species. The change in electrical resistance (or conductance) relative to the starting condition following exposure to a reducing or oxidizing gas component is the most common definition of sensitivity applied to solid state chemiresistive gas sensors [12]:

$$S = \frac{|\Delta R|}{R_o} \times 100\% = \frac{R_{gas} - R_{air}}{R_{air}} \times 100\% \qquad (2)$$

Where R is the electrical resistance, the subscripts (air) and (gas) denote that the analytic gas has been added and the backdrop is the initial dry air state, respectively.

Using inspect F-50 FESEM company, the morphology of the samples was studied. We measured the average crystallite size and crystal structure using XRD (6000 SHIMADZ). Perkin Elmer Spectrophotometer Model Lambda 365 UV absorption was measured using a twin beam with a wavelength range of 190–1100 nm.

Using a home-made gas-detection device, the sensors' sensing abilities were tested. Electrical feeds passed via the base plate. To heat the test sample and reach the necessary operating temperatures, the heating was adjusted on the base plate. A relay with adjustable ON/OFF time intervals was used to measure the current flowing through the heating element. To gauge the working temperature of the sensors, a thermocouple was employed. Digital temperature indicators were linked to the thermocouple's output. At one port of the base plate, a gas inlet valve was installed. By employing a gas flow meter to inject a known volume of test gas, the required gas concentration inside the system was reached. A digital millimeter was used to measure current while a steady voltage was delivered to the sensors. Following each Gases exposure cycle, air was permitted to enter the chamber.

Result and discussion

Figure (1) displays the thin film XRD patterns that were produced by typical spray pyrolysis. the samples were prepared on glass substrate at temperature 400°C ,30cm distance between spray head and substrate and The scans were performed over 2ɵ = 10° - 90° . In general, we can find that the sample had a polycrystalline structure and all of the observed peaks can be assigned to the sample, in accordance to the data obtained from JCPDF NO. 96-900-9087. X-ray diffraction patterns for (TiO2) thin film exhibit a polycrystalline nature having (101), (004), (200), (211), (204), Tetragonal anatase-phased planes with nanostructure. Full width at half maximum (FWHM), interplanar distance (dhkl), and grain size (G.S.) are represented in Table 1. The Scherrer equation is used to calculate the grain size from the full width at half maximum (FWHM) (β) of the best

orientation diffraction peak [13]. According to the findings, nanocrystalline TiO2 material can be generated under favorable conditions. A better crystallization of the materials is indicated by smaller grains and larger FWHN values.

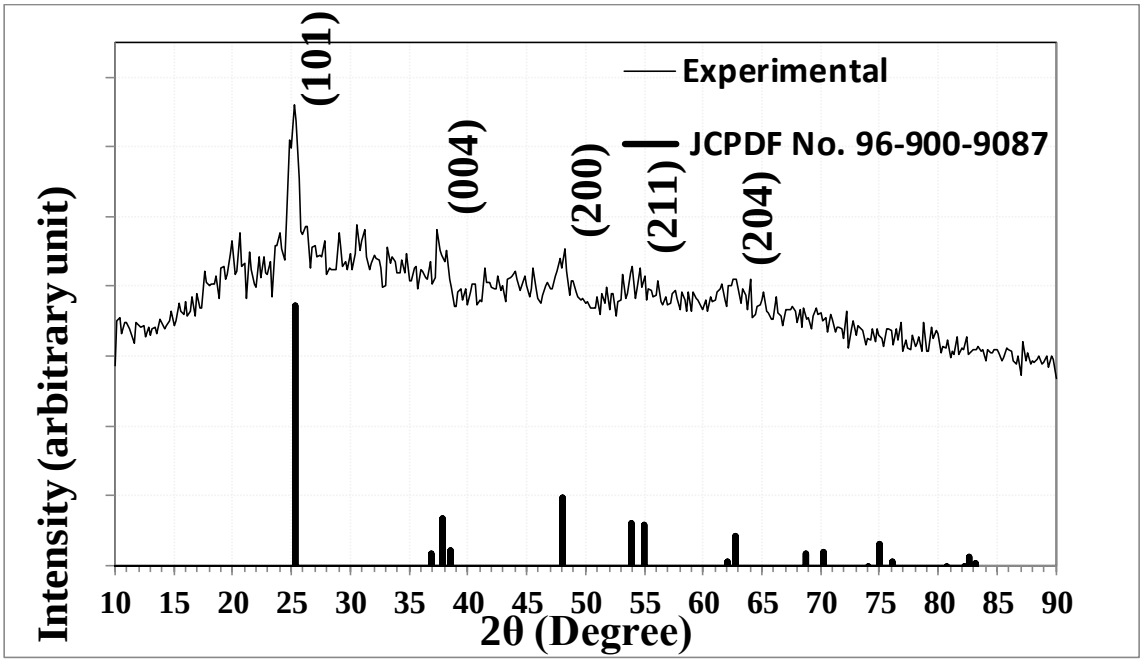

Figure (1): XRD of pure TiO2 thin films on glass substrate .

Table (1) the Experimental value of TiO_2 parameters for the peaks showed in XRD.

2θ (Deg.)	FWHM (Deg.)	d_{hkl} (Å)	D (nm)	Phase	hkl
25.26	0.9437	3.5235	8.6	Anatase TiO_2	(101)
37.52	1.0485	2.3950	8.0	Anatase TiO_2	(004)
48.22	1.1009	1.8858	7.9	Anatase TiO_2	(200)
54.25	1.4155	1.6896	6.3	Anatase TiO_2	(211)
62.63	1.2057	1.4820	7.7	Anatase TiO_2	(204)

On the FESEM image, nanoscale grass-like structures are seen in the TiO2 thin film of figure (2). The nanostructure exhibits alignment and uniform (with few voids) distribution. Additionally, the surface has polyhedral shells that are scattered unevenly across the substrate, some of which align with the nanoparticles. The SEM image displays uniform distribution of tiny granular grains over the surface without any fissures. There were small, spherical granules that ranged in size from 21.39 to 39.93 nm. The surface of the film seems to be homogeneous and free of holes or cracks. The grain size, however, is less than what was predicted from the FESEM surface micrograph, according to XRD data.

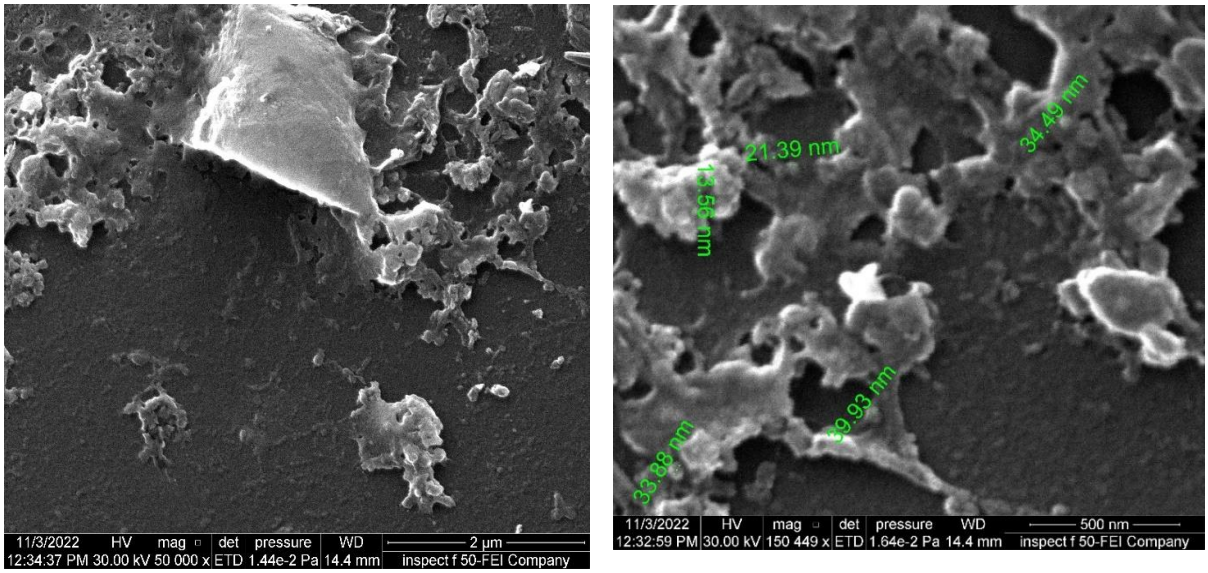

Figure (2) The FESEM images of pure TiO2 thin film deposited on glass substrate.

In Figure 3, it is demonstrated how produced films were optically measured using UV-Vis. The thin-film absorbance spectra as a function of wavelengths between 300 and 900 nm. These oscillations are a sign of good optical quality in the films because they were transparent, uniformly adhered to the substrate, and stable for a long time when exposed to air. Over the wavelength range of 400 to 800 nm, the thin film's average transmission had a lower absorbance of roughly 0.1. Pure TiO2 semiconductor thin films at the absorption edge are responsible for a dramatic decrease in absorption at about 375 nm.

The data point close to the absorption edge can be used to calculate the semiconductor's band gap (E_g). Figure 3(b) displays how $(\alpha h\upsilon)^2$ changes in relation to $(h\upsilon)$. The sample's optical energy gap is roughly 3.3 eV.

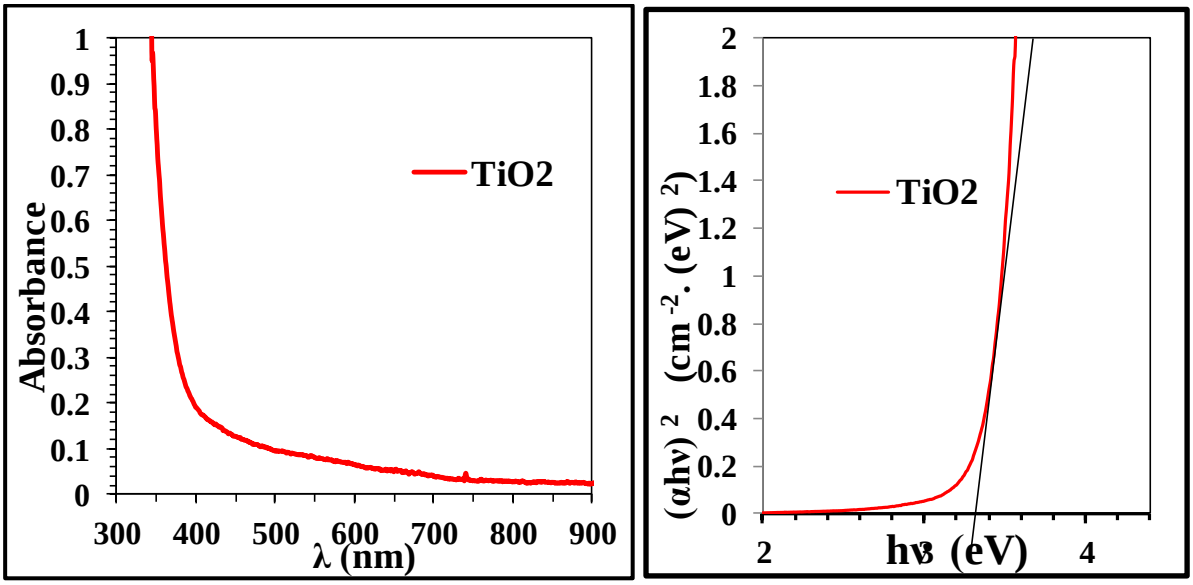

Figure 3 (a) transmission spectrum as a function of wavelength for pure TiO2 (b) (αhn)² as a function of hn for pure TiO2 .

The semiconducting properties of thin films is verified through testing. The thin film is positioned on the heater, and resistances are measured in the dry air environment between (RT up to 200 0C). Figure (4) depicts how the resistance of pure (TiO2) thin films on glass substrate varies with temperature. The Arrhenius equation governs how the resistance changes with temperature[14]. Due to the characteristics of oxide semiconductors, the films exhibit high resistance at low working temperatures, and their resistance decreased as the operating temperature rose.

Shows a typical negative temperature coefficient for resistance that results from charge carriers heat stimulation in semiconductors [14][15]. As temperature rises over 200 oC, thin films exhibit a resistance-positive temperature coefficient. This is explained by the conduction band filling up with electrons from oxygen vacancies' shallow donor levels. At this point, an increase in temperature causes an electron's mobility to decrease, which causes the resistance to rise. There is a temperature range where changes in temperature have little of an impact on the resistance of films because of the sensor's little temperature dependence. This is likely because equilibrium has been reached between the two competing processes of thermal excitation of electrons and oxygen adsorption[15].

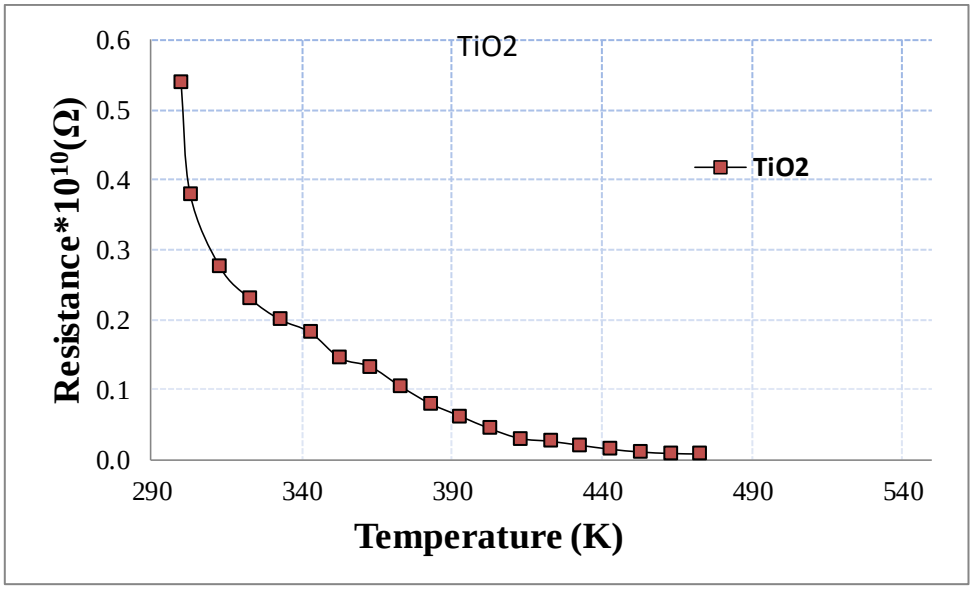

Figure 4: The variation of resistance with temperature of the pure TiO_2 , on glass substrate.

The oxidation state of the metal component (the oxide's stoichiometry) and the type and amount of mixture used to create the thin films are key determinants of the oxide semiconductors' electrical characteristics. The concentration (n) and mobility (μ) of the appropriate free carrier affect electrical conductivity (σ). For the production of thin films

with high conductivity, high carrier concentration and mobility must coexist [16]. Also, the morphology of the samples has a significant impact on the electrical properties[17].

Oxygen vacancy concentration increases electrical conductivity [18]. With less input from the grain boundary, nanometric grains exhibit better electrical conductivity. In this case, the high (σ) is related to the homogeneous distribution of the carriers through the grain, differently from the non-nanosized grains in which the (σ) is associated to trapped carriers in the grain boundary[19]. Only a small portion of the total conductivity is affected by the grain border, with the majority of the electrical conductivity being impacted by the mobility of electrons within the grain.

When temperatures are low, the charge mobility of carriers, which is dependent on the defect/dislocation concentration, is what causes conductivity to increase. Low temperature zone conduction is the name given to the conduction process in most cases. Due to a modest amount of thermal energy that is more than sufficient to activate the charge carriers that occur during the conduction process, the activation energy during this area grows as the operation temperature for samples rises and has a maximum value. While the rise in charge mobility is responsible for the increase in conductivity in the low temperature area. The activation energy is higher in high temperature areas than it is in low temperature areas. In this area, intrinsic flaws have a significant role in determining electrical conductivity.

Table (2): The Activation energy of pure TiO_2

sample	Ea1 (eV)	Range (K)	Ea2 (eV)	Range (K)	σRT *10-7(Ω-1.cm-1)
pure TiO2	0.18641	303-393	0.37779	393-473	33.06878307

Figure (5) depicts the temperature dependence of the sensitivity of a pure TiO_2 gas sensor coated on a glass substrate for NO_2 and H_2S gases at operating temperatures (200, 250, and 300 °C) using a reducing gas (H_2S) with a concentration of 30 ppm and an oxidizing gas (NO_2) with a concentration of 60 ppm. This figure demonstrates that. At the required working temperature of 200 to 300 °C, both gases have good sensitivity. It should be noted that the maximum sensitivity for 60 ppm NO_2 for temperatures up to 300°C was around 51.1%, but the higher sensitivity to 30 ppm from H_2S was approximately 52.4%. The nano-sized and greater quantity of can be used to explain the improved sensitivity.

The response and recovery times of the pure TiO_2 gas sensor samples for NO_2 and H_2S gases are shown in Table (3) as functions of temperature. The results of the sample response and recovery times are shown in the table for each gas, and it can be seen that as the operation temperature rises, the sample response and recovery times also do as well. Whereas at 250°C operation temperature, pure TiO_2 has a quick response time of 18s for

H_2S gas. For H_2S gas, however, at an operating temperature of 300°C, the recovery period is quick (42.3s).

The surface reaction between chemisorbed oxygen and oxide gas is a key component of the gas sensing mechanism. There are two ways that oxygen can adsorb on a film surface: physisorption and chemisorption. Chemisorption predominates at high temperatures. Increasing operational temperature can provide the activation energy necessary for the switch from physisorption to chemisorption. According to reports, as the temperature rises, the amount of oxygen adsorbed on the sensor surface also rises [20][21]. At temperatures between 200 and 300 °C, when the oxygen is adsorbed at the surface of the metal oxide that allows an electron trapping, both molecular oxygen and atomic oxygen have a dominant influence on the electrophysical and gas sensing features of samples. Thus, the charge carrier density is decreased, which causes the resistance of pure and mixed samples to increase. The creation of a depletion layer that extends to the particles as well as the surface barrier is caused by O^- species on the surface acting as electron acceptors. Since it regulates the electron transfer between particles, test gas, and the sensing material, and so affects the overall resistance, these surface states and surface barriers play a significant role for sensors. Exposure to NO_2 gas, with an elevated temperature, the preadsorbed oxygen species ($O^- surf$). It causes the oxygen coverage to increase, attracting more electrons to the samples' conduction band and thereby boosting the barrier. As a result of this phenomena, the conductivity is decreased or the resistance is increased [22].

Figure (6) displays how pure TiO2's resistance changes over time when it is subjected to H2S and NO2 in the ambient air introduced into the testing chamber. When the gas is opened to allow for mixing with the chamber's air, the sensor resistance achieves its steady state before the resistance is directly measured with time. As soon as the gas is turned on, the resistance changes abruptly to attain a stable condition before returning to its original value. The type of contact between the gas molecules and the surface atoms of the detecting film determines whether a sensor can detect the presence of gas. The structural flaw has a significant impact on the surface's responsiveness. When the gas is on, the resistance increases quickly and eventually reaches saturation. This could be because the surface has become saturated with H2S gas adsorption. When the gas is turned off, the resistance returns to its initial state. When exposed to NO2 gas, the resistance rapidly decreases.

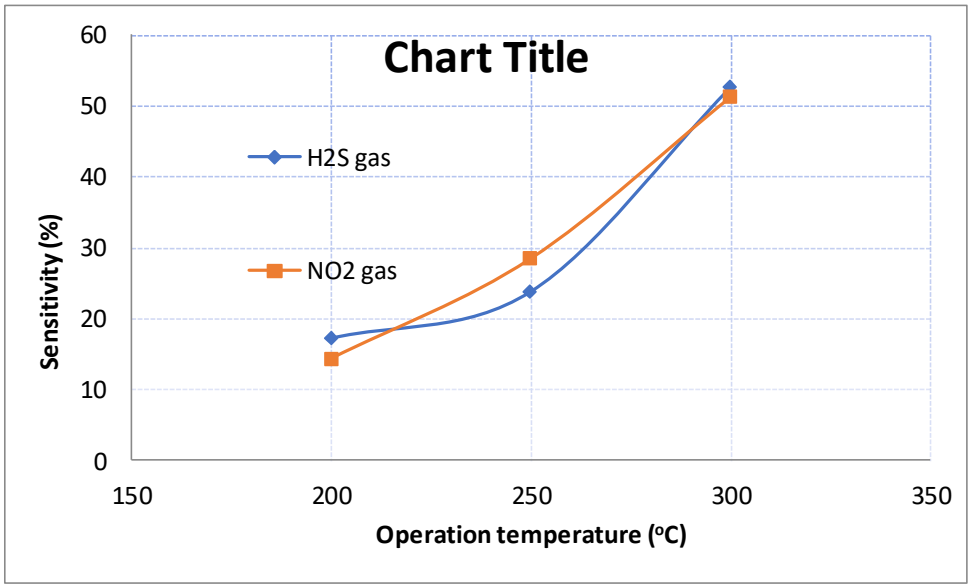

Figure (5): The variation of sensitivity with the operating temperature of the prepared pure TiO2 to H_2S and NO_2 gases.

Table (3): response time and recovery time with operation temperature of the prepared TiO2 to H_2S and NO_2 gases.

	NO2 gas		H2S gas	
Temperature C	response time(sec)	recover time (sec)	response time(sec)	recover time (sec)
200	23.4	66.6	19.8	63
250	25.2	64.8	18	50.4
300	26.1	45.9	27.9	42.3

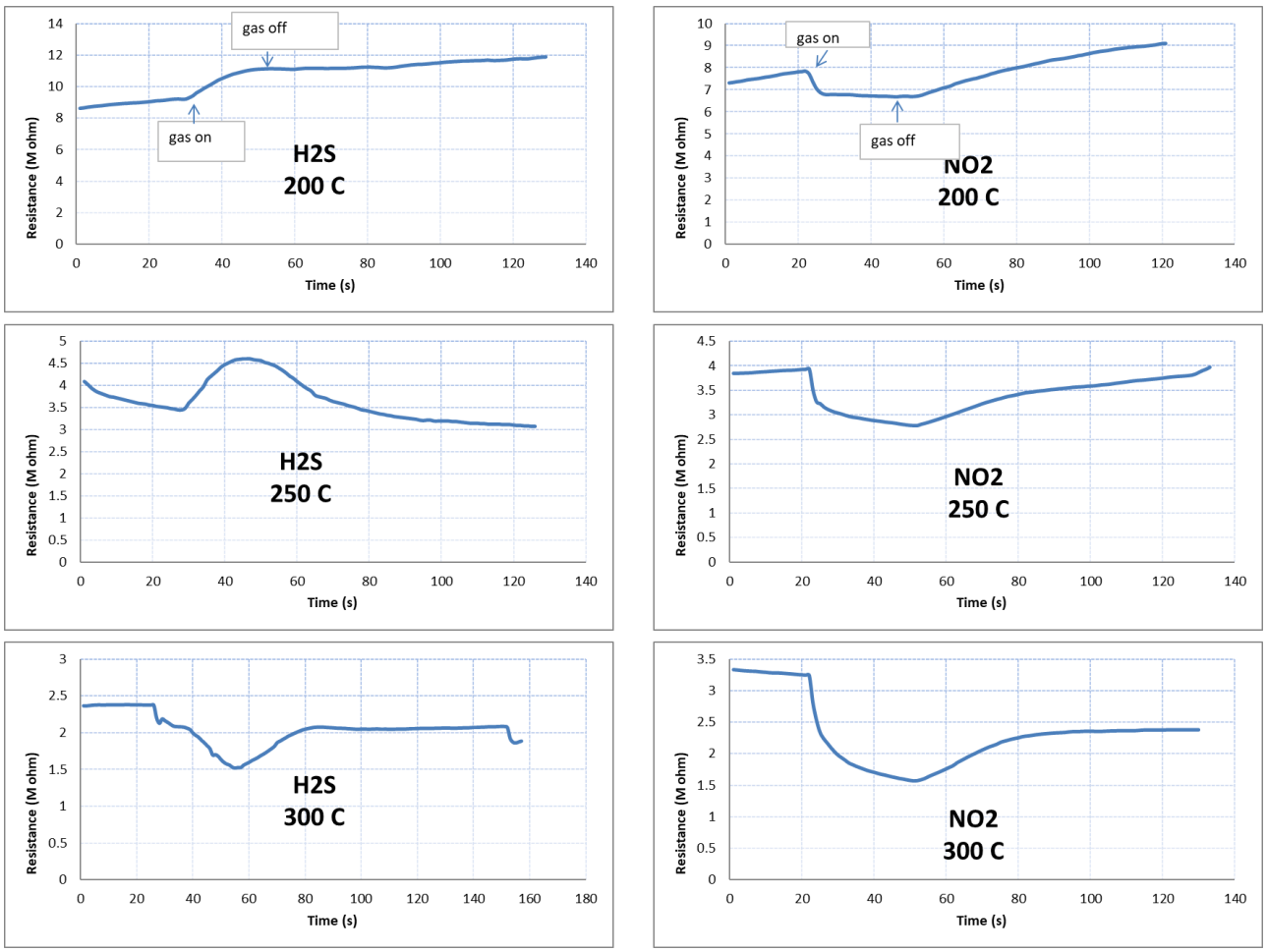

Figure (6): The variation resistance with time for different operation temperature of NO_2 and H_2S gases for the pure TiO2 gas sensor.

Conclusion

This work successfully demonstrated how spray pyrolysis, a straightforward and affordable method, could be used to create TiO_2 thin films. SEM and XRD have shown the presence of nanoparticles with average sizes and the nanostructured nature of the surface, respectively. The behavior of TiO2 thin films as displayed in the provided graphs had demonstrated that the films were having higher sensitivity and low response and recovery time which were indicated for H2S and NO2 gas sensing device.

Reference

[1] L. G. González *et al.*, "Synthesis and characterization of nanostructured TiO2 and TiO2/W thin films deposited by co-sputtering," *Rev. Mater.*, vol. 23, no. 2, Jul. 2018, doi: 10.1590/s1517-707620180002.0401.

[2] T. Chemical and E. Journal, "High-Efficiency Dye-Sensitized Solar Cells Based on Nitrogen and Graphene oxide co- incorporated TiO2 nanofibers photoelectrode," no. January 2015, 2016, doi: 10.1016/j.cej.2015.01.065.

[3] D. Rafieian, W. Ogieglo, T. Savenije, and R. G. H. Lammertink, "Controlled formation of anatase and rutile TiO2 thin films by reactive magnetron sputtering Controlled formation of anatase and rutile TiO 2 thin films by reactive magnetron sputtering," vol. 097168, no. 2015, 2017, doi: 10.1063/1.4931925.

[4] M. P. Moret, R. Zallen, D. P. Vijay, and S. B. Desu, "Brookite-rich titania films made by pulsed laser deposition," *Thin Solid Films*, vol. 366, no. 1–2, pp. 8–10, May 2000, doi: 10.1016/S0040-6090(00)00862-2.

[5] J. Osterwalder, T. Droubay, T. Kaspar, J. Williams, C. M. Wang, and S. A. Chambers, "Growth of Cr-doped TiO2 films in the rutile and anatase structures by oxygen plasma assisted molecular beam epitaxy," *Thin Solid Films*, vol. 484, no. 1–2, pp. 289–298, 2005, doi: 10.1016/j.tsf.2005.02.028.

[6] Y. C. Liang, N. C. Xu, and K. J. Chiang, "Surface Morphology-Dependent Functionality of Titanium Dioxide–Nickel Oxide Nanocomposite Semiconductors," *Nanomater. 2019, Vol. 9, Page 1651*, vol. 9, no. 12, p. 1651, Nov. 2019, doi: 10.3390/NANO9121651.

[7] Z. Zhou *et al.*, "Effects of annealing conditions and multifold morphology on photocatalytic properties of TiO2 nanorods," *Appl. Phys. A Mater. Sci. Process.*, vol. 129, no. 1, pp. 1–9, 2023, doi: 10.1007/s00339-022-06321-2.

[8] R. Azpiroz, E. Carretero, A. Cueva, A. González, M. Iglesias, and J. J. Pérez-Torrente, "In-flow photocatalytic oxidation of NO on glasses coated with nanocolumnar porous TiO2 thin films prepared by reactive sputtering," *Appl. Surf. Sci.*, vol. 606, no. October, 2022, doi: 10.1016/j.apsusc.2022.154968.

[9] M. Siva Prasad, R. Chen, H. Ni, and K. Kiran Kumar, "Directly grown of 3D-nickel oxide nano flowers on TiO2 nanowire arrays by hydrothermal route for electrochemical determination of naringenin flavonoid in vegetable samples," *Arab. J. Chem.*, vol. 13, no. 1, pp. 1520–1531, 2020, doi: 10.1016/j.arabjc.2017.12.004.

[10] S. G. Ullattil and P. Periyat, "Sol-Gel Synthesis of Titanium Dioxide," Springer, Cham, 2017, pp. 271–283. doi: 10.1007/978-3-319-50144-4_9.

[11] A. M. More, J. L. Gunjakar, and C. D. Lokhande, "Liquefied petroleum gas (LPG) sensor properties of interconnected web-like structured sprayed TiO2 films," *Sensors Actuators, B Chem.*, vol. 129, pp. 671–677, 2008, doi: 10.1016/j.snb.2007.09.026.

[12] L. A. Patil, A. R. Bari, M. D. Shinde, V. V. Deo, and D. P. Amalnerkar, "Synthesis of

ZnO nanocrystalline powder from ultrasonic atomization technique, characterization, and its application in gas sensing," *IEEE Sens. J.*, vol. 11, no. 4, pp. 939–946, 2011, doi: 10.1109/JSEN.2010.2066265.

[13] D. Rusu, G. Rusu, and D. Luca, "Structural characteristics and optical properties of thermally oxidized Zinc films," *Acta Phys. Pol. A*, vol. 119, no. 6, pp. 850–856, 2011, [Online]. Available: http://przyrbwn.icm.edu.pl/APP/PDF/119/a119z6p21.pdf

[14] S. S. Kawar, "Development of Nanostructured Cadmium Oxide (Cdo) Thin Films Results And Discussion," vol. 1, no. 1, pp. 11–14, 2012.

[15] Asmaa N.Mohammed Ali, Abother Ghanim AL Mohana, Jinan Mohammed Abbas ,"Sructural and gptical properties of Fe_2O_3:CdTe thin films grown by pulse laser deposition at different X content" IV.International Scientific Congress of Pure , Applied and Technology Sciences (Minar Congress) (onlain Available) pp.364-371, (2021) https://dx.doi.org/10.47832/MinarCongress4-31.

[16] S. Calnan and a. N. Tiwari, "High mobility transparent conducting oxides for thin film solar cells," *Thin Solid Films*, vol. 518, no. 7, pp. 1839–1849, 2010, doi: 10.1016/j.tsf.2009.09.044.

[17] M. M. Rahman *et al.*, "Effect of Al Doping on Structural, Electrical, Optical and Photoluminescence Properties of Nano-Structural ZnO Thin Films," *J. Mater. Sci. Technol.*, vol. 28, no. 4, pp. 329–335, 2012, doi: 10.1016/S1005-0302(12)60064-4.

[18] H. M. Ali and M. Raaif, "Plasma oxidation of electron beam evaporated cadmium thin films," *Thin Solid Films*, vol. 520, no. 13, pp. 4418–4421, 2012, doi: 10.1016/j.tsf.2012.02.063.

[19] D. Lamb and S. J. C. Irvine, "Near infrared transparent conducting cadmium oxide deposited by MOCVD," *Thin Solid Films*, vol. 518, no. 4, pp. 1222–1224, 2009, doi: 10.1016/j.tsf.2009.05.067.

[20] P. Shankar, J. Bosco, and B. Rayappan, "Gas sensing mechanism of metal oxides : The role of ambient atmosphere , type of semiconductor and gases - A review ScienceJet," *Sci. Jet*, vol. 4, p. 126, 2015.

[21] R. R. Salunkhe, V. R. Shinde, and C. D. Lokhande, "Liquefied petroleum gas (LPG) sensing properties of nanocrystalline CdO thin films prepared by chemical route: Effect of molarities of precursor solution," *Sensors Actuators, B Chem.*, vol. 133, pp. 296–301, 2008, doi: 10.1016/j.snb.2008.02.024.

[22] Z. A. Ansari, T. G. Ko, and J.-H. O. J.-H. Oh, "CO-sensing properties of In_2O_3-doped SnO_2 thick-film sensors: effect of doping concentration and grain size," *IEEE Sens. J.*, vol. 5, no. 5, 2005, doi: 10.1109/JSEN.2005.854485.